# Visualization and analysis of single-cell RNA-seq data by kernel-based similarity learning

Bo Wang[1,+] (bowang87@stanford.edu)

Junjie Zhu[2] (jjzhu@stanford.edu)

Emma Pierson[1](emmap1@stanford.edu)

Serafim Batzoglou [1] (serafim@cs.stanford.edu)

[1] Department of Computer Science, Stanford University

[2] Department of Electrical Engineering, Stanford University

[+] To whom correspondence should be addressed. Email: bowang87@stanford.edu.

## Abstract

Single-cell RNA-seq technologies enable high throughput gene expression measurement of individual cells, and allow the discovery of heterogeneity within cell populations. Measurement of cell-to-cell gene expression similarity is critical to identification, visualization and analysis of cell populations. However, single-cell data introduce challenges to conventional measures of gene expression similarity because of the high level of noise, outliers and dropouts. Here, we propose a novel similarity-learning framework, SIMLR (**s**ingle-cell **i**nterpretation via **m**ulti-kernel **l**ea**r**ning), which learns an appropriate distance metric from the data for dimension reduction, clustering and visualization. We show that SIMLR separates subpopulations more accurately in single-cell data sets than do existing dimension reduction methods. Additionally, SIMLR demonstrates high sensitivity and accuracy on high-throughput peripheral blood mononuclear cells (PBMC) data sets generated by the GemCode single-cell technology from 10x Genomics.

**Keywords:** single-cell analysis, similarity learning, dimension reduction, data visualization

## Background

Single-cell RNA sequencing (scRNA-seq) technologies have recently emerged as a powerful means to measure gene expression levels of individual cells and to reveal previously unknown heterogeneity and functional diversity among cell populations [1]. Quantifying the variation across gene expression profiles of individual cells is key to the identification and analysis of complex cell populations that arise in neurology [2], immunology [3], oncology [4] and developmental biology [5]. The heterogeneity identified across individual cells can answer questions irresolvable by traditional ensemble-based methods, where gene expression measurements are averaged over a population of cells pooled together [6], [7]. Recent works have demonstrated that *de novo* cell type discovery and identification of functionally distinct cell subpopulations are possible via unbiased analysis of all transcriptomic information provided by scRNA-seq data [8]. Therefore, unsupervised clustering of individual cells using scRNA-seq DATA is critical to developing new biological insights and validating prior knowledge.

Most existing single-cell studies employ computational and statistical methods that have been developed primarily for analysis of data from traditional bulk RNA-seq methods [8]–[10]. These methods do not address the unique characteristics that make single-cell expression data especially challenging to analyze: outlier cell populations, transcript amplification noise, and biological effects such as the cell cycle [11]. In addition, it has been shown that many statistical methods fail to alleviate other underlying challenges, such as dropout events, where zero expression measurements occur due to sampling or stochastic transcriptional activities [12]. Recently, new single-cell platforms such as DropSeq [13], InDrop [14] and GemCode single-cell technology [15] have enabled a dramatic increase in throughput to thousands of cells. These platforms have adapted recent sequencing protocols such as unique molecular identifiers (UMIs)

to create digital counts of transcripts in a cell. However, with 3'-end sequencing instead of full transcript sequencing, low coverage per cell and varying capture efficiency, these high-throughput platforms produce data sets where 95% of measurements are zeros.

The technological differences across single-cell platforms as well as the biological differences across studies can strongly affect the usability of unsupervised clustering methods. Core to the problem is that unsupervised clustering methods usually rely on specific similarity metrics across the objects to be clustered, and standard similarity metrics may not generalize well across platforms and biological experiments, and thus be unsuitable for scRNA-seq studies. To address this problem and answer the key question of "which cells are similar or different" in a way that generalizes across different single-cell data sets, we introduce SIMLR (**s**ingle-cell **i**nterpretation via **m**ulti-kernel **l**ea**r**ning), a novel framework that learns appropriate cell-to-cell similarities from the single-cell data. We use SIMLR to simultaneously (1) cluster cells into groups for subpopulation identification and (2) produce a 2-D or 3-D visualization of the expression data. SIMLR preserves consistency between clustering and visualization, enabling one to quantitatively and qualitatively understand structures underlying single-cell data sets.

SIMLR offers two main advantages over previous methods: (1) it *learns* a distance metric that best fits the structure of the data. This is important because the diverse statistical characteristics of single-cell data produced today do not easily fit specific statistical assumptions made by standard dimension reduction algorithms; (2) in contrast to some previous analyses that pre-select gene subsets of known function [10], [16], SIMLR is unsupervised, thus allowing *de novo* discovery from the data. We empirically demonstrate that SIMLR produces more separable data points and more reliable clusters than PCA as well as many commonly used nonlinear methods,

and we use SIMLR to provide 2-D and 3-D visualizations that assist with the interpretation of single-cell data derived from several diverse technologies and biological samples.

## Results and Discussion

### Overview of Algorithm

Here we highlight the main ideas in our methodology underlying SIMLR, and we provide full details in **Materials and Methods**.

Given a $N \times M$ gene expression matrix $X$ with $N$ cells and $M$ genes ($N < M$) as an input, SIMLR solves for $S$, an $N \times N$ symmetric matrix that captures pairwise similarities of cells. In particular, $S_{ij}$, the $(i,j)^{\text{th}}$ entry of $S$, represents the similarity between cell $i$ and cell $j$. SIMLR assumes that if $C$ separable populations exist among the $N$ cells, then $S$ should have an approximate block-diagonal structure with $C$ blocks whereby cells have larger similarities to other cells within the same subpopulations.

We introduce an optimization framework that learns $S$ by incorporating multiple kernels to learn appropriate cell-to-cell distances from the data (**Figure 1a**). We provide an efficient algorithm to optimize for $S$, while simultaneously learning the block-diagonal structure within $S$. The cell-to-cell similarity values in $S$ can be used to create an embedding of the data in 2-D or 3-D for visualization, as well as a projection of the data into a latent space of arbitrary dimension to further identify groups of cells that are similar (**Figure 1b**).

*General optimization framework*

SIMLR computes cell-to-cell similarities through the following optimization framework:

$$\underset{S,L,w}{\text{minimize}} \quad \sum_{i,j} D(x_i, x_j) S_{ij} + \beta \|S\|_F^2 + \gamma\, \mathbf{tr}(L^T (I_N - S) L) + \rho \sum_l w_l \log w_l$$

$$\text{subject to } D(x_i, x_j) = \sum_l w_l D_l(x_i, x_j), \sum_l w_l = 1, w_l \geq 0, \tag{1}$$

$$L^T L = I_C, \sum_j S_{ij} = 1, \text{and } S_{ij} \geq 0 \text{ for all } (i, j),$$

where $x_i$ is the length-$M$ gene expression vector of cell $i$, i.e., the $i$th row of $X$; $D(x_i, x_j)$ is the distance between cell $i$ and cell $j$, expressed as a linear combination of distance metrics $D_l$ with weights $w_l$; $I_N$ and $I_C$ are $N \times N$ and $C \times C$ identity matrices respectively; and $\beta$ and $\gamma$ are non-negative tuning parameters. $\|S\|_F$ is the Frobenius norm of $S$. The optimization problem involves solving for three variables: the similarity matrix $S$, the weight vector $w$, and a $N \times C$ rank-enforcing matrix $L$.

The intuition behind the first term in the formula is that the learned similarity $S$ between two cells should be small if the distance between them is large. The second term is a regularization term that avoids over-fitting the model to the data. If there are $C$ subpopulations, the gene expressions of cells of the same sub-type should have high similarity, and ideally the effective rank of $S$ should be $C$. Thus, the third term along with the constraint on $L$ enforces the low-rank structure of $S$: the matrix $(I_N - S)$ is essentially the graph Laplacian [17], and the trace-minimization problem enforces approximately $C$ connected components in a similarity graph that consists of nodes representing the cells, and edge weights corresponding to pairwise similarity values in $S$ [17]. The fourth term imposes constraints on the kernel weights to avoid selection of a single kernel; we empirically found that this regularization improves the quality of learned similarity (Supplementary Table 1).

One critical component of this optimization problem is the choice of the distance measure $D(x_i, x_j)$ between pairs of cells. It is well-known that the distance metric defined for the input space is critical to the performance of clustering and visualization algorithms designed for high-dimensional data [18]. Due to the presence of outliers and unusual zero-inflated distributions in single-cell data, standard metrics like the Euclidian distance may fail to perform well. Thus, instead of using a pre-defined distance metric, we incorporate multiple kernel learning [19] that flexibly combines multiple distance metrics.

We employ an efficient algorithm for optimizing $S$, $L$ and $w$. The intuition behind our procedure is simple: holding two of these three variables fixed, the optimization problem over the third variable is convex. Hence, we alternate between optimizing each variable while holding the other two fixed until convergence (for full details, see **Materials and Methods**).

*Dimension reduction for clustering and visualization*

SIMLR relies on the stochastic neighbor embedding (SNE) [20] methodology for dimension reduction, with an important modification: t-SNE computes the similarity of the high-dimensional data points using a Gaussian kernel as a distance measure and projects the data onto a lower dimension that preserves this similarity. Instead of using the gene expression matrix as an input to t-SNE, we use the learned cell-to-cell similarities $S$ (detailed in **Supplementary Methods**).

For visualization, we use our modified t-SNE algorithm to project the data into two or three dimensions so that the hidden structures in the data can be depicted intuitively. For clustering, we use the same approach to reduce the dimensions to $B$, resulting in an $N \times B$ latent matrix $Z$, to

which we can apply any existing clustering algorithms, such as K-means [21] to assign labels to each cell. The number of reduced dimensions $B$ is typically equal to the number of desired clusters $C$.

## Applications

### *Cell-to-cell similarities*

We start by benchmarking SIMLR against conventional pre-defined measures in capturing true cell-to-cell similarities on four published single-cell data sets (for the full details of each data set, see **Materials and Methods**):

1. Eleven cell populations including neural cells and blood cells (Pollen data set [9]).
2. Neuronal cells with sensory subtypes (Usoskin data set [8]).
3. Embryonic stem cells under different cell cycle stages (Buettner data set [16]).
4. Pluripotent cells under different environment conditions (Kolodziejczk [10]).

We selected these data sets because they span a variety of cell types and have different numbers of subpopulations, representing a wide range of single-cell data; cell types in each dataset were also known *a priori* and were further validated in the respective studies, providing a reliable gold standard with which to assess clustering performance. To evaluate SIMLR's performance on these data sets, we compared subpopulation labels assigned after dimension reduction with SIMLR to the true subpopulation labels from the respective studies. **Table 1** summarizes the number of cells, genes and validated populations in each data set, as well as the run time of SIMLR on each data set.

SIMLR was given the raw gene expressions and the true number of clusters, but no information about the true labels. Once the similarities were computed, we organized the cells according to the known or validated cell populations (i.e., true labels) from each study. As is shown in **Figure 2**, we compared the cell-to-cell similarities learned by SIMLR with a similarity matrix computed from Gaussian kernels applied to Euclidean distances (Euclidean Similarity), and a pairwise correlation matrix (Pearson Correlation). Each column in **Figure 2** corresponds to a different data set and each row corresponds to a different kind of similarity. The axes of the symmetric matrices are colored and organized by the true labels.

As can be seen by comparing the rows of **Figure 2**, SIMLR learned a similarity matrix with block structures in remarkable agreement with the previously validated labels, while the other similarity matrices agree less well. Both Euclidean distances and Pearson correlations are sensitive to outliers, and Pearson correlations do not capture nonlinear relationships, so spurious similarities between cells from different groups surface with these pre-defined measures. On the other hand, SIMLR handles outliers with its rank constraint and nonlinear similarities using multiple kernels, making its learned similarity more suitable for single-cell data sets.

Furthermore, SIMLR demonstrates one additional advantage: it can identify additional subpopulation structures even when the number of clusters input into the algorithm is conservatively selected. From the similarity structure learned by SIMLR in the Kolodziejczyk data set in **Figure 2**, we observed that each of the three validated clusters could be further divided into sub-clusters, which is consistent with the unsupervised analysis in the corresponding study [10]. However, these sub-clusters were identified using a small number of pre-selected genes in the original study. SIMLR preserved these substructures in an unbiased fashion while having clearly removed the spurious similarities between cells from different (validated) groups.

(In the remainder of our analysis, as gold standard we use only the unbiased and validated true labels as opposed to the additional subpopulations identified by unsupervised analysis.)

*Clustering Performance Metrics*

The similarity matrix learned by SIMLR can be leveraged to reduce the dimension of the original data for clustering. Many other dimension reduction approaches have been applied upstream of various clustering methods. For a more systematic analysis of SIMLR's performance, we compared it to other dimension reduction methods using two types of metrics.

First, we assume only the number of clusters is known *a priori* and run K-means on the dimension-reduced data in order to group cells into clusters; we compare this clustering to the true clustering using the normalized mutual information (NMI), a standard measure of clustering concordance. Second, we classify each cell based on the true labels of its nearest neighbors in the dimension-reduced space, and assess the accuracy of this classification using cross validation; we refer to this metric as nearest neighbor error (NNE). This test assesses how accurately new cells can be classified using cells whose labels are already known. (The formal mathematical definitions of NMI, NNE and other cluster performance metrics are provided in **Supplementary Notes**.)

We select these two performance metrics because they measure different aspects of the data in the low dimensional latent space: NNE directly reflects how closely cells from the same population are surrounded by each other, whereas NMI provides a global view of how well cells from different populations are separated. We also tested four other performance metrics in

**Supplementary Notes**, shown in **Supplementary Figures 2-5**, to ensure that SIMLR performed well under different standards.

*Comparison with other dimension reduction methods*

We performed extensive comparisons of SIMLR with 8 other methods on the four data sets to test its utility. The 8 methods included standard linear methods including PCA [22], FA [33], and probabilistic PCA (PPCA) [28]; nonlinear methods including t-SNE [23], Laplacian eigenmaps [25], multidimensional scaling (MDS) [26], and Sammon mapping [27]; and model-based methods specifically designed for single-cell data like zero-inflated factor analysis (ZIFA) [12]. The methods we tested included all methods used in analyses of the original data sets. In addition, the Pollen and the Usoskin data sets were the only ones with validated labels used in [12] to assess ZIFA, which was specifically designed for single-cell data.

The NMI and NNE values for the 9 methods are summarized in **Table 1** and **Table 2** respectively. Our method consistently outperforms the existing alternatives on the four data sets, and most of the differences in NMI and NNE between SIMLR and the second best method are remarkably large.

To test the robustness of SIMLR, we conducted three additional experiments for each data set.

1. We used varying numbers (3 - 20) of latent dimensions $B$ to evaluate the performance of SIMLR and other methods. This evaluation is critical because typically the true number of clusters in the data is unknown. (As mentioned before, ideally $B$ should be equal to the true number of clusters for SIMLR.)

2. We dropped varying fractions (5% - 70%) of the gene measurements in the input gene expression matrix to analyze how each method performs when random levels of dropout are present across the data, which is relevant to the high dropout rate in single-cell data.
3. We added independent zero-mean Gaussian noise with varying variances $\sigma^2$ (0.1 – 1) to the gene expression matrix. The number of dimensions $C$ used in this experiment is set to be the true number of clusters. In order to preserve the dropout characteristics, we ensured that the added noise was set to zero at a frequency equal to the dropout rate in each data set. Formally, we added a random noise vector $y_i$ to $x_i$ by the following process:

$$z_i \sim \text{Normal}(0, \sigma^2 I_M), \qquad h_{ij} \sim \text{Bernoulli}(p_0), \qquad y_{ij} = \begin{cases} z_{ij}, \text{if } h_{ij} = 0 \\ 0, \text{if } h_{ij} = 1 \end{cases} \qquad (2)$$

where $p_0$ is the dropout rate (proportion of zeros) in the original expression matrix $X$. We set the values of an entry in the new expression matrix to zero if its value after adding noise dropped below zero.

The NMI and NNE values (**Figure 3a, b)** on the Buettner data set show remarkably better performance by SIMLR as compared to other methods. In addition, we observe that SIMLR is not sensitive to the number of latent dimensions $B$ even though the most suitable choice of $B$ should ideally be the number of clusters if it is known. ZIFA and FA achieve high NMI values at certain values of $B$ but are less stable and can perform much worse than SIMLR otherwise (as is shown in the first column of **Figure 3**). Moreover, as the fraction of genes increases, the NMI increases and the NNE decreases more noticeably for SIMLR. Finally, while the performance of SIMLR decreases with the noise variance, it still outperforms other methods.

Based on other metrics on all four data sets (shown in **Supplementary Figures 2-5**), we observe that SIMLR also outperforms other methods in a similar fashion and no other method dominates

in specific regimes. Therefore, SIMLR should be considered a safe alternative to existing approaches for single-cell data sets that are generally similar to the four data sets we consider.

*Visualization of cells in 2-D*

After confirming that cell-to-cell similarities learned by SIMLR are meaningful and that the clustering performance of SIMLR is reliable, we applied SIMLR's SNE-based dimension reduction to 2-D to verify that the structures in the data are visually intuitive. We compared SIMLR with two of the most commonly used visualization methods in single-cell analysis: PCA and t-SNE. We also included ZIFA, which was shown to outperform many other model-based methods [15]. In **Figure 4**, none of the four methods used the true labels as inputs for dimension reduction, and we only added the true label information (in the form of distinct colors) afterwards to validate the results.

SIMLR successfully separates the clusters for the Pollen (11 populations) and the Buettner (3 populations) data sets, whereas other methods contain clusters that are mixed to different extents. For the 3 populations in the Kolodziejczyk data set, SIMLR and t-SNE perform similarly and separate the clusters more clearly than PCA and ZIFA. For the 4 populations in Usoskin, none of the methods separated the clusters completely but SIMLR and tSNE exhibit less overlap than PCA and ZIFA. These results indicate that SIMLR overall uncovers meaningful clusters that are more identifiable than those produced by existing methods. The visualizations of the four data sets using other dimension reduction methods are provided in **Supplementary Figure 1** for reference.

*Application to sparse PBMC data sets*

Single-cell RNA-seq data produced from high-throughput microfluidics platforms such as DropSeq [13], InDrop [14] and GemCode single-cell technology [15] contains up to 95% zero expression counts. We tested the performance of SIMLR on sparse datasets by applying it to PBMC scRNA-seq data from the GemCode [15]. The PBMC data were from 5 bead enriched populations: naïve B (CD19+ and IgD+), CD56+ natural killer (NK) cells, CD8+ cytotoxic T cells, CD4+ T cells and CD14+ monocytes. The purity of the populations was validated by FACS, and clustering analysis of the scRNA-seq transcriptome profile. To generate a ground truth set, we generated *in silico* mixtures from these 5 datasets at specific proportions: 10%, 5%, 25%, 40%, 20%. SIMLR provided an unbiased classification of these subpopulations that was highly consistent (with NMI over 0.95 on average). In addition, we used t-SNE and PCA with K-means clustering as baselines, and they also produced good agreement with the true labels **(Figure 5a)**. The overall improvement of SIMLR over t-SNE and PCA was noticeable but not highly significant because many cell types (such as monocytes, naïve B cells) are easily distinguishable from other cell types.

To provide intuition for how SIMLR differs from t-SNE and PCA, we illustrate one of the trials (**Figure 5b-c,** colored by ground-truth cell types) where the 5 different cell types are better separated using SIMLR. PCA produced the most ambiguous visualization across NK cells, CD8+ cytotoxic T cells and CD4+ T cells, whereas t-SNE did not completely separate NK cells from CD8+ cytotoxic T cells. We performed pairwise clustering to elucidate the cases where SIMLR and other methods differ (**Figure 5d** and **Supplementary Figure 7**). While most pairs were easy to separate by all methods, SIMLR's overall improvement over t-SNE and PCA resulted from its ability to separate CD8+ T cells and NK cells (highlighted in the orange boxes

in **Figure 5e**). CD8+ T cells and NK cells are difficult to separate because the two cell types can share several common gene markers and certain T cells share properties of both NK and CD8+ cells [23], [24]. In the case where SIMLR did not outperform PCA (highlighted in the blue boxes in **Figure 5d**), we found that SIMLR mistakenly grouped a very small number of monocytes with NK cells but still correctly separated the vast majority, leading to a negligible difference from PCA.

No clustering method is guaranteed to always outperform others on real data sets, especially when the number of clusters is sometimes difficult to pre-determine. For this reason, each method can have a certain degree of variability. Using the *in silico* mixing of immune cells, we showed that SIMLR can still reveal reliable clusters on sparse data sets and the overall performance is indeed insensitive to the variability from trial to trial.

*Simulation on simulated nonlinear manifold data sets*

In addition to real single-cell data sets with ground truth information, we evaluated SIMLR's performance on simulated data to evaluate how accurately it captured nonlinear manifolds. We focused on comparisons to t-SNE because SIMLR directly adapts the algorithm for t-SNE. We first created artificial clusters of cells (concentric circles) in a low-dimensional latent space (**Figure 6a**), used a random linear transformation to project the data into a high dimensional space, and then added noise and zeros following the model in [12] to create the single-cell gene expression matrix. (More details on the simulation methodology are provided in **Supplementary Notes**.) In **Figure 6b,** we show how SIMLR separates the clusters more clearly than t-SNE, as measured by NNE (results were similar with other metrics; **Supplementary Figure 7**) at each stage of the data generation process: prior to adding noise or zeros, after adding noise, and after adding zeros. When more noise (**Figure 6c**) or dropouts (**Figure 6d**) are added to the data, the

cluster information in t-SNE becomes obscured, where as the impact on SIMLR is less significant as the NNE is lower and the clusters are still separated very well.

While in this example we generate clusters as concentric circles in the latent space to illustrate how SIMLR can separate even clusters with complex structures, we also evaluated SIMLR's performance on Gaussian clusters (**Supplementary Figures 9 and 10**), comparing to factor analysis and ZIFA [12] as well as to t-SNE. We found that SIMLR outperformed the other methods if the dropout rate was low, whereas ZIFA outperformed the other methods if the dropout rate was high; the latter result is unsurprising, because ZIFA is explicitly designed to accommodate a high dropout rate and we generated the data using ZIFA's dropout model.

## Conclusions

High-throughput single-cell RNA sequencing technologies have enabled fine-grained analysis of cell-to-cell heterogeneity and molecular functions within tissues and cell populations that until recently could only be studied in bulk. As additional high-throughput approaches become available for single-cell RNA-seq, a wider range of studies pertaining to fundamental cellular functions will continue to emerge. Consequently, single-cell data sets may exhibit even higher levels of diversity (e.g., different tissues, comparisons of healthy versus disease-associated cell populations, different stages of the cell cycle or across development, different experimental technologies, and other sources of variation across data sets). Such diversity in experimental conditions and cell collections makes it difficult and undesirable to define cell-to-cell similarity measures based on strict statistical assumptions. As novel methodologies and algorithms are urgently needed for this new type of data, SIMLR can adapt to the heterogeneity across different single-cell data sets by learning an appropriate similarity measure for each data set.

In this paper we extensively evaluated SIMLR using recently published distinct single-cell data sets and without any prior knowledge of groups of significant genes. We demonstrated that SIMLR is able to learn appropriate cell-to-cell distances that uncover similarity structures that would otherwise be shadowed by noise or outlier effects. Furthermore, SIMLR successfully clusters cell populations and projects the high-dimensional data in a visually intuitive fashion. We show that SIMLR separates clusters more cleanly than 8 other popular dimension reduction methods, including linear methods (such as PCA), nonlinear methods (such as Sammon), and a recently published approach (ZIFA) specifically designed for single-cell data sets [12].

Because each dimension reduction algorithm makes its own assumptions, it is unlikely that one is optimal for all data sets. As we have shown, SIMLR performs very well on single-cell data

sets that contain several clusters -- a frequent use case where heterogeneity is defined by distinct cell lineages. But because SIMLR assumes the data has cluster structures, it may not be best suited for data that does not contain clear clusters, such as cell populations that contain cells spanning a continuum. Further, because SNE-based algorithms (such as SIMLR) generally preserve local rather than global structure of the data, they may be best suited for problems where local structure (such as clustering) is of interest rather than continuous global structure (such as progression through pseudotime). Similar to many non-linear methods (such as t-SNE), SIMLR scales quadratically with the number of cells during similarity computation. This scalability limits the utility of SIMLR, as well as most unsupervised methods, when the number of cells is large, even though it runs very quickly on most available single-cell data sets. Therefore, when it comes to single-cell data sets with a very large number of cells, modifications to SIMLR will be necessary. For these applications, it would be computationally tractable to first apply SIMLR to a subset of cells, and then use the labeled cells to train a classifier to identify the remaining cells. Such an approach with other clustering methods have been used several single-cell studies [13][25] to make the computation feasible. It would be interesting to extend SIMLR in this direction to explore the tradeoff between the number of cells used for the initial clustering and the sensitivity in identifying rare cell populations. Advances in both experimental and computational approaches for single-cell analysis will lead to new and fundamental discoveries in areas spanning important biological systems.

## Materials and Methods

### Four Published Data Sets

For all the data sets above, we applied a logarithmic transformation $f(X) = \log_{10}(X + 1)$ to the single-cell raw expression data. We used the following four data sets in our analysis:

1. Eleven cell populations including neural cells and blood cells (Pollen data set [9]). This data set was designed to test the utility of low-coverage single-cell RNA-seq in identifying distinct cell populations, and thus contained a mixture of diverse cell types: skin cells, pluripotent stem cells, blood cells, and neural cells. This data set includes samples sequenced at both high and low depth; we analysed the high-depth samples, which were sequenced to an average of 8.9 million reads per cell.
2. Neuronal cells with sensory subtypes (Usoskin data set [8]). This data set contains 622 cells from the mouse dorsal root ganglion, with an average of 1.14 million reads per cell. The authors divided the cells into four neuronal types: peptidergic nociceptors, non-peptidergic nociceptors, neurofilament containing, and tyrosine hydroxylase containing.
3. Embryonic stem cells under different cell cycle stages (Buettner data set [16]). This data set was obtained from a controlled study that quantified the effect of the cell cycle on gene expression level in individual mouse embryonic stem cells (mESCs). An average of 0.5 million reads were obtained for each of the 182 cells and at least 20% of the reads were mapped to known exons on the mm9 mouse genome. The cells were sorted for three stages of the cell cycle using fluorescence-activated cell sorting, and were validated using gold-standard Hoechst staining.
4. Pluripotent cells under different environment conditions (Kolodziejczyk data set [10]). This data set was obtained from a stem cell study on how different culture conditions

influence pluripotent states of mESCs. This study quantified the expression levels of about 10 thousand genes across 704 mESCs from 9 different experiments involving three different culture conditions. An average of 9 million reads were obtained for each cell and over 60% of the reads mapped to exons on the *Mus musculus* genome.

**Five Purified Immune Cell Types in Human PBMC**

scRNA-seq libraries of 5 bead-enriched PBMC populations were generated by 10x Genomics [15]. We computationally sampled a total of 1000 cells randomly from the individual purified populations at the proportion of 10%, 5%, 25%, 40%, 20%, respectively for each *in silico* trial after selecting cells by total UMI counts (**Supplementary Figure 6**).

**Multiple Kernel Learning**

Instead of using a predefined distance metric, we incorporate multiple kernel learning in SIMLR to compute the distances between pairs of cells. The general form of the distance between cell $i$ and cell $j$ is defined as

$$D(c_i, c_j) = \sum_l w_l \, D_l(c_i, c_j) = \sum_l w_l \, \|\phi_l(c_i) - \phi_l(c_j)\|_2^2 \tag{3}$$

where $\phi_l(c_i)$ is the $l$th kernel-induced *implicit* mapping of the $i$th cell. This mapping is implicit because we are only concerned about the inner products of the $\phi_l(c_i)$ and $\phi_l(c_j)$ for pairs $(i, j)$ as follows:

$$\begin{aligned} \|\phi_l(c_i) - \phi_l(c_j)\|_2^2 &= \phi_l(c_i)^T \phi_l(c_i) + \phi_l(c_j)^T \phi_l(c_j) - 2\phi_l(c_i)^T \phi_l(c_j) \\ &= K_l(c_i, c_i) + K_l(c_j, c_j) - 2\, K_l(c_i, c_j) = 2 - 2\, K_l(c_i, c_j) \end{aligned} \tag{4}$$

where we only need to compute the kernel functions: $K_l(c_i, c_j)$. (The kernel of two identical inputs is set to 1 by convention). So we can refine the optimization problem to include the distance in the objective and the corresponding weights as variables as follows.

$$\begin{aligned} \underset{S,L,w}{\text{minimize}} \quad & -2\sum_{i,j,l} w_l K_l(c_i, c_j) S_{ij} + \beta \|S\|_F^2 + \gamma\, \mathbf{tr}(L^T(I_N - S)L) + \rho \sum_l w_l \log w_l \\ \text{subject to} \quad & L^T L = I_C, \sum_l w_l = 1, w_l \geq 0, \sum_j S_{ij} = 1, \text{and } S_{ij} \geq 0 \end{aligned} \tag{5}$$

We describe the optimization of $L$, $w$, and $S$ below; we describe selection of the parameters $\beta, \gamma$ and $\rho$ in the **Supplementary Methods.**

**Solving the optimization problem**

Initialization of $S, w,$ and $L$: The weight of multiple kernels, $w$, is initialized as an uniform distribution vector, i.e., $w = \left(\frac{1}{G}, \frac{1}{G}, \ldots, \frac{1}{G}\right)$, where $G$ is the number of kernels. This uniform weights suggests that we don't have any bias towards any specific kernel. The similarity matrix $S$ is initialized as $S_{ij} = \sum_l w_l K_l(c_i, c_j)$ . $L$ is initialized as the top $B$ eigenvectors of $S$.

The optimization problem formulated above is non-convex with respect to all of the variables $S, L, w$, but the problem of each variable conditional on other variables being fixed is convex. So we can apply an alternating convex optimization method to solve this tri-convex problem efficiently. The following three steps are implemented iteratively until the variables all converge. The update schemes are shown in Algorithm (1).

Notice that Step 4 is an auxiliary step in this problem where we incorporate a similarity enhancement heuristic that can further improve clustering accuracy. The similarity obtained from Equation (4) is usually sparse because of the constraints, so some pairwise interactions can be absent even though they can be exploited by higher order structures such as local connectivity. So we create a diffusion process where we can improve the similarities.

*Step 1: Fixing $L$ and $w$ to update $S$:*

When we minimize the objective function with respect to (w.r.t.) the similarity matrix $S$, we can rewrite the optimization problem as follows.

$$\begin{aligned} \underset{S}{\text{minimize}} \quad & -\sum_{i,j}\left[\sum_{l} w_l K_l(c_i, c_j) + \gamma (LL^T)_{ij}\right] S_{ij} + \beta \|S\|_F^2 \\ \text{subject to} \quad & \sum_{j} S_{ij} = 1 \text{ and } S_{ij} \geq 0 \text{ for all } (i,j) \end{aligned} \tag{6}$$

The first summation term in the objective as well as constraints are all linear, and the second summation in the objective is a simple quadratic form that can be solved in polynomial time [26].

*Step 2: Fixing $S$ and $w$ to update $L$:*

When we minimize the objective function w.r.t. the latent matrix $L$, we can rewrite the optimization problem as follows.

$$\begin{aligned} \underset{L}{\text{maximize}} \quad & \mathbf{tr}(L^T(S - I_N)L) \\ \text{subject to} \quad & L^T L = I_C \end{aligned} \tag{7}$$

The trace of $L^T(S - I_N)L$ is maximized when $L$ is an orthogonal basis of the eigenspace

associated with the $C$ largest eigenvalues of $(S - I_N)$ [27]. Thus, $L$ can be computed efficiently using any matrix numeric toolbox.

*Step 3: Fixing S and L to update w:*

When we minimize the objective function w.r.t. the kernel weights $w$, we can re-write the optimization problem as follows.

$$\begin{aligned} \underset{w}{\text{maximimize}} \quad & \sum_l w_l \sum_{i,j} K_l(c_i, c_j) S_{ij} - \rho \sum_l w_l \log w_l \\ \text{subject to} \quad & \sum_l w_l = 1, w_l \geq 0, \end{aligned} \tag{8}$$

The problem with a convex objective and linear constraints can be solved by any standard convex optimization method quickly [26]. Details of steps in updating $w$ and choices the multiple kernels are stated in **Supplementary Methods**.

*Step 4: Similarity enhancement*

Given a similarity matrix $S$, we construct a transition matrix $P$ such that

$$P_{ij} = \frac{S_{ij}\, \mathbf{1}_{\{j \in A_K(i)\}}}{\sum_l S_{il}\, \mathbf{1}_{\{l \in A_K(i)\}}}, \tag{9}$$

where $A_K(i)$ represents the set of indices of cells that are the $K$ top neighbors of cell $i$ under the learned distance metric. Under this construction, the transition matrix is sparse as well so we preserve most of the similarity structure. The diffusion-based method to enhance the similarity S has the following update scheme:

$$H_{ij}^{(t+1)} = \tau H_{ij}^{(t+1)} P + (1 - \tau) I_N \tag{10}$$

where we have $H_{ij}^{(0)} = S_{ij}$ as an input and the final iteration of $H_{ij}$ is used as the new similarity measure $S_{ij}$. We show that the diffusion process converges in **Supplementary Methods**.

SIMLR iterates the four steps above until convergence. We use the eigengap (**Supplementary Methods**) as the convergence criterion. When the method has converged, the similarity S should be stable and so its eigengap, i.e, the difference between the $C + 1$th and $C$th eigenvalues, should be stable too. Further, a good low rank similarity $S$ should have a small eigengap. We show the dynamics of the eigengap during iterations in SIMLR on the four real data sets (**Supplementary Figure 11**). SIMLR converges within around 10 iterations.

## Additional File

The following additional file is available with this paper. Additional file 1: **Supplementary Information** includes Supplementary Notes, Figures and Methods.

## Abbreviations

SIMLR: Single-cell Interpretation via multi-kernel enhanced similarity learning; mESCs: mouse embryonic stem cells; NMI: Normalized mutual information; NNE: Nearest neighbor error; MDS: Multidimensional scaling; FA: Factor analysis; PCA: Principal component analysis; PPCA: Probabilistic principal components analysis; ZIFA: Zero-inflated factor analysis; SNE: Stochastic neighbor embedding; t-SNE: t-distributed stochastic neighbor embedding.

## Competing interests

SB is co-founder of DNAnexus and member of the scientific advisory boards of 23andMe, Genapsys and Eve Biomedical.

## Authors' contributions

BW, JZ and SB conceived the study and planned experiments. BW developed algorithms and software implementation. BW, JZ and EP performed data analysis and implemented the simulation study. JZ and EP drafted the manuscript. BW and SB contributed to the manuscript. All authors read and approved the final manuscript.

## Acknowledgements

The authors would like to thank Grace X Zheng, Jessica Terry, Tarjei Mikkelsen from 10x Genomics for providing access to the PBMC data as well as suggestions for the manuscript and the *in silico* experiments.

## References


[1] E. Shapiro, T. Biezuner, and S. Linnarsson, "Single-cell sequencing-based technologies will revolutionize whole-organism science," *Nat. Rev. Genet.*, vol. 14, no. 9, pp. 618–630, 2013.

[2] E. Llorens-Bobadilla, S. Zhao, A. Baser, G. Saiz-Castro, K. Zwadlo, and A. Martin-Villalba, "Single-Cell Transcriptomics Reveals a Population of Dormant Neural Stem Cells that Become Activated upon Brain Injury," *Cell Stem Cell*, vol. 17, no. 3, pp. 329–340, Jul. 2015.

[3] A. K. Shalek, R. Satija, X. Adiconis, R. S. Gertner, J. T. Gaublomme, R. Raychowdhury, S. Schwartz, N. Yosef, C. Malboeuf, D. Lu, J. J. Trombetta, D. Gennert, A. Gnirke, A. Goren, N. Hacohen, J. Z. Levin, H. Park, and A. Regev, "Single-cell transcriptomics reveals bimodality in expression and splicing in immune cells.," *Nature*, vol. 498, no. 7453, pp. 236–40, Jun. 2013.

[4] N. E. Navin, "Delineating cancer evolution with single-cell sequencing," *Sci. Transl. Med.*, vol. 7, no. 296, pp. 296fs29–296fs29, 2015.

[5] M. S. Kowalczyk, I. Tirosh, D. Heckl, T. Nageswara Rao, A. Dixit, B. J. Haas, R. Schneider, A. J. Wagers, B. L. Ebert, and A. Regev, "Single cell RNA-seq reveals changes in cell cycle and differentiation programs upon aging of hematopoietic stem cells.," *Genome Res.*, p. gr.192237.115–, Oct. 2015.

[6] R. Sandberg, "Entering the era of single-cell transcriptomics in biology and medicine," *Nat. Methods*, vol. 11, no. 1, pp. 22–24, 2014.

[7] N. E. Navin, "Cancer genomics: one cell at a time," *Genome Biol.*, vol. 15, no. 8, p. 452,

2014.

[8] D. Usoskin, A. Furlan, S. Islam, H. Abdo, P. Lönnerberg, D. Lou, J. Hjerling-Leffler, J. Haeggström, O. Kharchenko, P. V Kharchenko, S. Linnarsson, and P. Ernfors, "Unbiased classification of sensory neuron types by large-scale single-cell RNA sequencing," *Nat. Neurosci.*, vol. 18, no. 1, pp. 145–153, 2014.

[9] A. a Pollen, T. J. Nowakowski, J. Shuga, X. Wang, A. a Leyrat, J. H. Lui, N. Li, L. Szpankowski, B. Fowler, P. Chen, N. Ramalingam, G. Sun, M. Thu, M. Norris, R. Lebofsky, D. Toppani, D. W. Kemp, M. Wong, B. Clerkson, B. N. Jones, S. Wu, L. Knutsson, B. Alvarado, J. Wang, L. S. Weaver, A. P. May, R. C. Jones, M. a Unger, A. R. Kriegstein, and J. a a West, "Low-coverage single-cell mRNA sequencing reveals cellular heterogeneity and activated signaling pathways in developing cerebral cortex," *Nat. Biotechnol.*, vol. 32, no. August, pp. 1–37, 2014.

[10] A. A. Kolodziejczyk, J. K. Kim, J. C. H. Tsang, T. Ilicic, J. Henriksson, K. N. Natarajan, A. C. Tuck, X. Gao, M. Bühler, P. Liu, J. C. Marioni, and S. A. Teichmann, "Single Cell RNA-Sequencing of Pluripotent States Unlocks Modular Transcriptional Variation," *Cell Stem Cell*, vol. 17, no. 4, pp. 471–485, 2015.

[11] D. Grün, L. Kester, and A. van Oudenaarden, "Validation of noise models for single-cell transcriptomics," *Nat. Methods*, vol. 11, no. 6, pp. 637–640, 2014.

[12] E. Pierson and C. Yau, "ZIFA: Dimensionality reduction for zero-inflated single-cell gene expression analysis," *Genome Biol.*, vol. 16, no. 1, p. 241, Nov. 2015.

[13] E. Z. Macosko, A. Basu, R. Satija, J. Nemesh, K. Shekhar, M. Goldman, I. Tirosh, A. R. Bialas, N. Kamitaki, E. M. Martersteck, J. J. Trombetta, D. A. Weitz, J. R. Sanes, A. K.

Shalek, A. Regev, and S. A. McCarroll, “Highly Parallel Genome-wide Expression Profiling of Individual Cells Using Nanoliter Droplets,” *Cell*, vol. 161, no. 5, pp. 1202–1214, 2015.

[14] A. M. Klein, L. Mazutis, I. Akartuna, N. Tallapragada, A. Veres, V. Li, L. Peshkin, D. A. Weitz, and M. W. Kirschner, “Droplet Barcoding for Single-Cell Transcriptomics Applied to Embryonic Stem Cells,” *Cell*, vol. 161, no. 5, pp. 1187–1201, May 2015.

[15] G. X. Y. Zheng, J. M. Terry, P. Belgrader, P. Ryvkin, Z. Bent, R. Wilson, S. B. Ziraldo, T. D. Wheeler, G. P. McDermott, M. T. Gregory, J. Shuga, L. Montesclaros, D. A. Masquelier, S. Y. Nishimura, M. Schnall-Levin, P. W. Wyatt, C. M. Hindson, R. Bharadwaj, A. Wong, K. D. Ness, L. W. Beppu, H. J. Deeg, C. McFarland, K. R. Loeb, W. J. Valente, N. G. Ericson, E. A. Stevens, J. P. Radich, T. S. Mikkelsen, B. J. Hindson, and J. H. Bielas, “Massively parallel digital transcriptional profiling of single cells,” *submitted*.

[16] F. Buettner, K. N. Natarajan, F. P. Casale, V. Proserpio, A. Scialdone, F. J. Theis, S. A. Teichmann, J. C. Marioni, and O. Stegle, “Computational analysis of cell-to-cell heterogeneity in single-cell RNA-sequencing data reveals hidden subpopulations of cells,” *Nat. Biotechnol.*, vol. 33, no. 2, pp. 155–160, 2015.

[17] U. von Luxburg, “A tutorial on spectral clustering,” *Stat. Comput.*, vol. 17, no. 4, pp. 395–416, Aug. 2007.

[18] E. P. Xing, A. Y. Ng, M. I. Jordan, and S. Russell, “Distance Metric Learning , with Application to Clustering with Side-Information,” *Adv. Neural Inf. Process. Syst.*, vol. 15, pp. 505–512, 2002.

[19] F. R. Bach, G. R. G. Lanckriet, and M. I. Jordan, "Multiple kernel learning, conic duality, and the SMO algorithm," in *Twenty-first international conference on Machine learning - ICML '04*, 2004, p. 6.

[20] G. E. Hinton and S. T. Roweis, "Stochastic neighbor embedding," in *Advances in neural information processing systems*, 2002, pp. 833–840.

[21] C. Ding and X. He, "K -means clustering via principal component analysis," in *Twenty-first international conference on Machine learning - ICML '04*, 2004, p. 29.

[22] I. Jolliffe, *Principal component analysis*. Wiley Online Library, 2002.

[23] P. G. Chu and D. A. Arber, "CD79: a review," *Appl. Immunohistochem. Mol. Morphol.*, vol. 9, no. 2, pp. 97–106, 2001.

[24] L. Van Kaer, "Regulation of immune responses by CD1d-restricted natural killer T cells," *Immunol. Res.*, vol. 30, no. 2, pp. 139–153, 2004.

[25] E. D. Amir, K. L. Davis, M. D. Tadmor, E. F. Simonds, J. H. Levine, S. C. Bendall, D. K. Shenfeld, S. Krishnaswamy, G. P. Nolan, and D. Pe'er, "viSNE enables visualization of high dimensional single-cell data and reveals phenotypic heterogeneity of leukemia," *Nat. Biotechnol.*, vol. 31, no. 6, pp. 545–552, 2013.

[26] Y. Nesterov, A. Nemirovskii, and Y. Ye, *Interior-point polynomial algorithms in convex programming*, vol. 13. SIAM, 1994.

[27] B. N. Parlett, *The symmetric eigenvalue problem*, vol. 7. SIAM, 1980.

## Figure Legends

### Figure 1

Outline of SIMLR. **(a)** SIMLR learns a proper metric for the cell-to-cell distances using the gene expression and constructs a similarity matrix. **(b)** The similarity matrix is used for visualization of cells in 2-D and for dimension reduction for clustering.

### Figure 2

Heatmaps of similarities of cells in four data sets. Three types of similarities are compared: (1) similarities learned from the data by SIMLR, (2) similarities computed from Gaussian kernels applied to Euclidean distances, and (3) similarities computed from pairwise Pearson correlations.

### Figure 3

Comparison of 9 different dimension reduction methods under the three robustness experiments on the Buettner data set. **(a)** The clustering accuracy in terms of NMI; higher scores denote better performance. **(b)** The clustering accuracy in terms of NNE; lower scores denote better performance. SIMLR is not sensitive to the number of latent dimensions selected for the algorithm (left column), and still outperforms other methods even when fractions of genes are dropped (middle column) or when additional noise is added to the data (right column).

### Figure 4

Comparison of different representative dimension reduction methods for visualizing four single-cell data sets. Each row corresponds to one of four different methods (SIMLR, t-SNE, PCA, and ZIFA) and each column corresponds to a different data set ([8]–[10], [16]). Each point is colored

by its true label in the corresponding data set. There are 3 labels for the Buettner data set, 11 for the Pollen data set, 3 for the Kolodziejczyk data set, and 4 for the Usoskin data set.

**Figure 5**

Comparison of SIMLR, tSNE and PCA for visualizing and clustering the PBMC data set. **(a)** NMIs, Accuracy, Rand Index (RI) and adjusted Rand Index (aRI) between true cell identity and cluster labels for each method over 20 trials of randomly sampling 1000 cells from 5 immune cell populations at a fixed proportion. **(b-d)** 2D visualization with **(b)** PCA **(c)** SIMLR and **(d)** t-SNE for a single trial where scatter points are colored by true cell labels. **(e)** Pairwise comparison plots for a single trial where the row and column of a plot specifies the two cell populations (indicated on the diagonal) being compared. Plots in the upper triangle show the NMIs associated with SIMLR, tSNE and PCA in clustering two different cell populations. Plots in the lower triangle show the 2-D projection of pairs of cell types using SIMLR, where points in grey are of the cell type defined by the row and those in purple are of the cell type defined by the column.

**Figure 6**

Dimension reduction of artificial gene expression generated from **(a)** 2-D latent data; each cluster is a concentric circle in the latent space. **(b)** The first row of plots show SIMLR's 2-D dimension reductions and the second row of plots show t-SNE's before adding noise or dropout (left plot), after adding noise (middle plot) and after adding noise and dropout (right plot). **(c)** NNE of t-SNE and SIMLR as noise is increased; lower scores denote better performance. **(d)**

NNE of of t-SNE and SIMLR as zeros are added to the data (smaller values of $\lambda$ indicate a higher dropout rate). **(e)** Fraction of entries zeroed out as a function of $\lambda$.

## Tables

**Table 1** Summary of the characteristics of the four real single-cell data sets, with SIMLR's computational time.

| Data set | # cells | # genes | # populations | run time (seconds) |
|---|---|---|---|---|
| **Pollen** [9] | 249 | 9966 | 11 | 3.40 |
| **Usoskin** [8] | 622 | 15332 | 4 | 18.54 |
| **Buettner** [16] | 182 | 9573 | 3 | 2.369 |
| **Kolodziejczyk [10]** | 704 | 11235 | 3 | 23.67 |

**Table 2.** NMI values for the four single-cell data sets. Higher values indicate better performance.

| Data set | PCA | Laplacian | MDS | t-SNE | Sammon | PPCA | FA | ZIFA | SIMLR |
|---|---|---|---|---|---|---|---|---|---|
| **Buettner** | 0.56 | 0.27 | 0.56 | 0.32 | 0.05 | 0.59 | 0.67 | 0.65 | 0.89 |
| **Kolodziejczyk** | 0.77 | 0.62 | 0.77 | 0.77 | 0.40 | 0.76 | 0.72 | 0.72 | 0.95 |
| **Pollen** | 0.83 | 0.80 | 0.83 | 0.93 | 0.75 | 0.83 | 0.82 | 0.79 | 0.94 |
| **Usoskin** | 0.39 | 0.48 | 0.39 | 0.69 | 0.41 | 0.40 | 0.36 | 0.41 | 0.69 |

**Table 3.** NNE values for the four single-cell data sets. Lower values indicate better performance.

| Data set | PCA | Laplacian | MDS | t-SNE | Sammon | PPCA | FA | ZIFA | SIMLR |
|---|---|---|---|---|---|---|---|---|---|
| **Buettner** | 0.21 | 0.38 | 0.22 | 0.18 | 0.21 | 0.20 | 0.11 | 0.16 | 0.05 |
| **Kolodziejczyk** | 0.0016 | 0.0278 | 0.0016 | 0.0014 | 0.018 | 0.0016 | 0.009 | 0.01 | 0.0018 |
| **Pollen** | 0.052 | 0.156 | 0.055 | 0.023 | 0.11 | 0.056 | 0.075 | 0.075 | 0.020 |
| **Usoskin** | 0.30 | 0.11 | 0.29 | 0.072 | 0.20 | 0.29 | 0.31 | 0.28 | 0.063 |

## Algorithms

**Algorithm 1** Similarity Learning via SIMLR

Input: $X$, the single-cell gene expression matrix, $C$, a target number of cell populations
Step 1 : Fix $L$ and $w$ to update $S$.
Step 2 : Fix $S$ and $w$ to update $L$.
Step 3 : Fix $L$ and $S$ to update $w$.
Step 4 : Enhance the similarity $S$.
Step 5 : Repeat 1-4 until $L$, $S$ and $w$ converge.

**Figure 1**

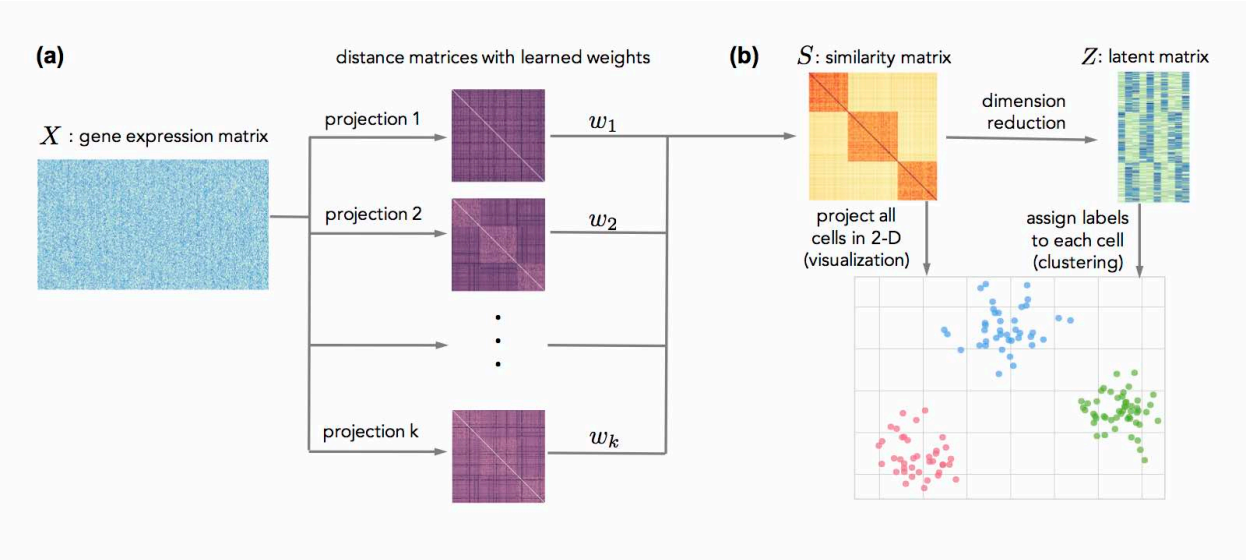
(a)
distance matrices with learned weights
(b)
$S$: similarity matrix
$Z$: latent matrix
$X$ : gene expression matrix
projection 1
projection 2
projection k
$w_1$
$w_2$
$w_k$
dimension reduction
project all cells in 2-D (visualization)
assign labels to each cell (clustering)

**Figure 2**

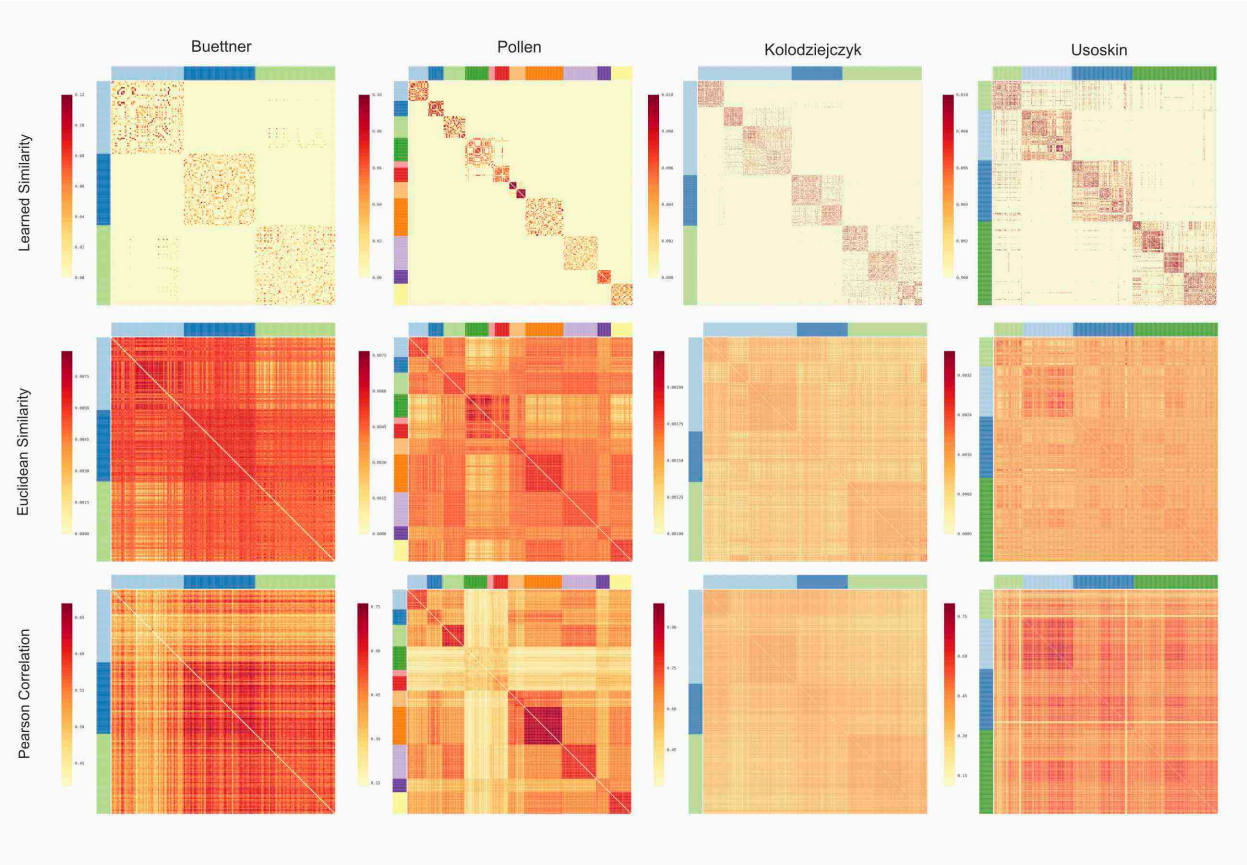
Buettner
Pollen
Kolodziejczyk
Usoskin
Learned Similarity
Euclidean Similarity
Pearson Correlation

**Figure 3**

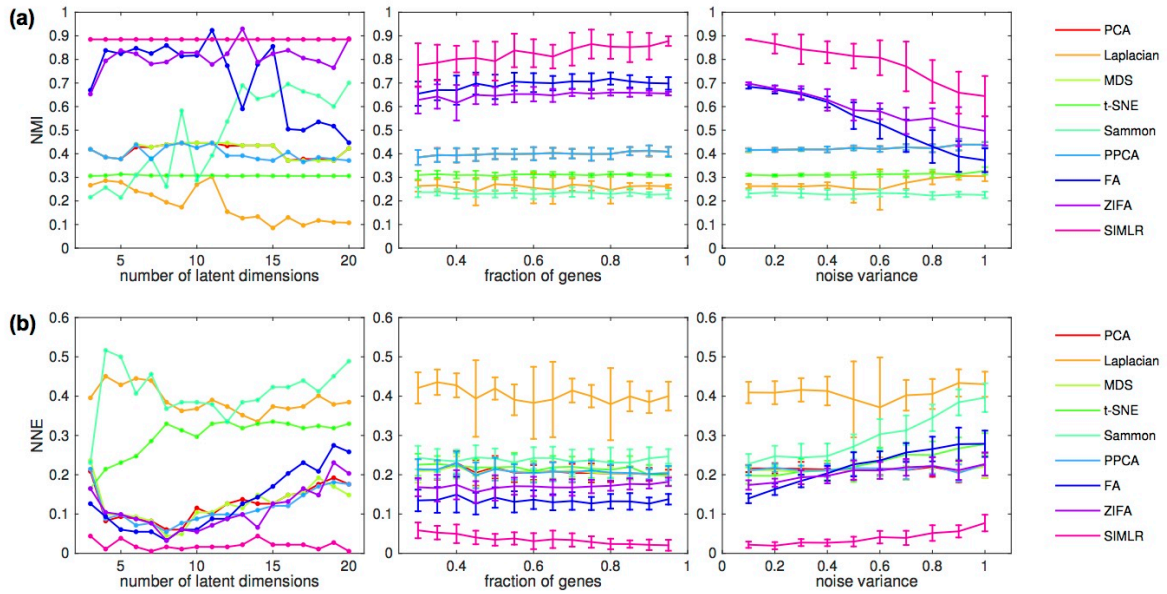
(a)
NMI
number of latent dimensions
fraction of genes
noise variance
PCA
Laplacian
MDS
t-SNE
Sammon
PPCA
FA
ZIFA
SIMLR
(b)
NNE
number of latent dimensions
fraction of genes
noise variance
PCA
Laplacian
MDS
t-SNE
Sammon
PPCA
FA
ZIFA
SIMLR

**Figure 4**

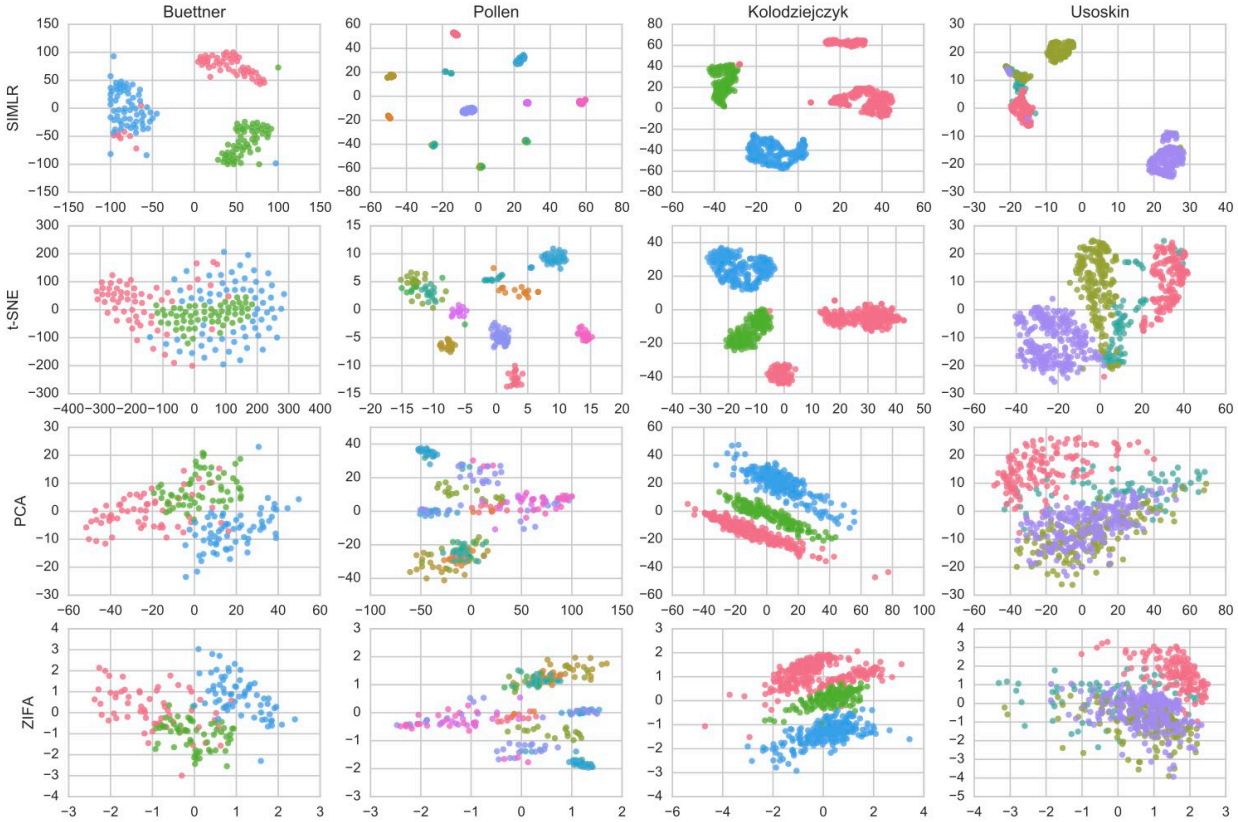
Buettner
Pollen
Kolodziejczyk
Usoskin
SIMLR
t-SNE
PCA
ZIFA

# Figure 5

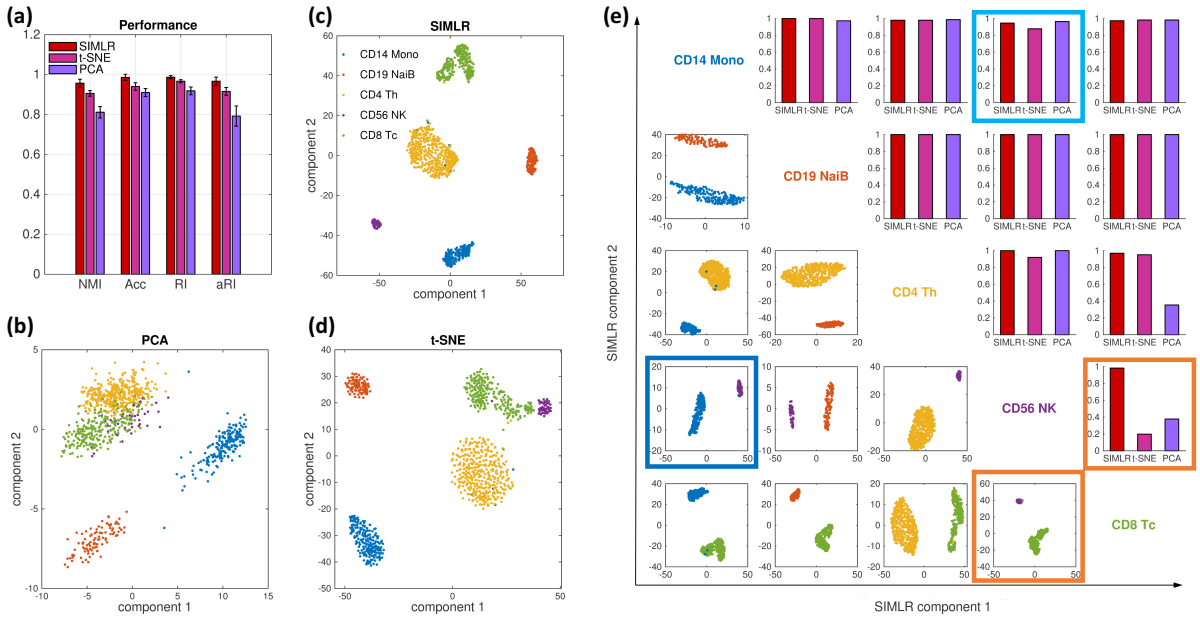
(a)
Performance
SIMLR
t-SNE
PCA
NMI
Acc
RI
aRI
(b)
PCA
component 1
component 2
(c)
SIMLR
CD14 Mono
CD19 NaiB
CD4 Th
CD56 NK
CD8 Tc
component 1
component 2
(d)
t-SNE
component 1
component 2
(e)
CD14 Mono
CD19 NaiB
CD4 Th
CD56 NK
CD8 Tc
SIMLR component 1
SIMLR component 2

**Figure 6**

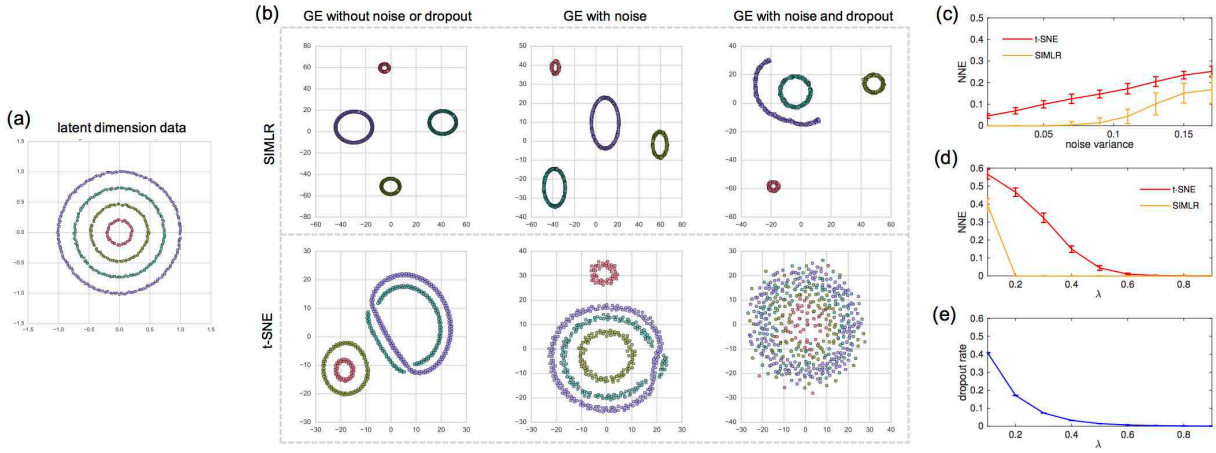
(a)
latent dimension data
(b)
GE without noise or dropout
GE with noise
GE with noise and dropout
SIMLR
t-SNE
(c)
t-SNE
SIMLR
NNE
noise variance
(d)
t-SNE
SIMLR
NNE
λ
(e)
dropout rate
λ